Time-Frequency Modulation Diversity To Combat Periodic Impulsive Noise In Narrowband Powerline Communications

Jing Lin, *Member, IEEE,* Tarkesh Pande, *Senior Member, IEEE,* Il Han Kim, *Member, IEEE,* Anuj Batra, *Senior Member, IEEE,* and Brian L. Evans, *Fellow, IEEE*

***Abstract*—Non-Gaussian noise/interference severely limits communication performance of narrowband powerline communication (PLC) systems. Such noise/interference is dominated by periodic impulsive noise whose statistics varies with the AC cycle. The periodic impulsive noise statistics deviates significantly from that of additive white Gaussian noise, thereby causing dramatic performance degradation in conventional narrowband PLC systems. In this paper, we propose a robust transmission scheme and corresponding receiver methods to combat periodic impulsive noise in OFDM-based narrowband PLC. Towards that end, we propose (1) a time-frequency modulation diversity scheme at the transmitter and a diversity demodulator at the receiver to improve communication reliability without decreasing data rates; and (2) a semi-online algorithm that exploits the sparsity of the noise in the frequency domain to estimate the noise power spectrum for reliable decoding at the diversity demodulator. In the simulations, compared with a narrowband PLC system using Reed-Solomon and convolutional coding, whole-packet interleaving and DBPSK/BPSK modulation, our proposed transceiver methods achieve up to 8 dB gains in E_b/N_0 with convolutional coding and a smaller-sized interleaver/deinterleaver.**

***Index Terms*—Periodic impulsive noise, narrowband powerline communications, modulation diversity, sparse Bayesian learning**

I. Introduction

Powerline communication (PLC) is a technology that sends data over electric power lines. Thanks to the widespread availability of power line infrastructure, PLC has been considered as a low-cost solution for smart grid communications. In particular, narrowband PLC operating in the 3–500 kHz band has gained tremendous interest for enabling communications between smart meters and data concentrators that are deployed by local utilities on low-voltage or medium-voltage power lines [1]. The applications include automatic meter reading, device-specific billing, time-dependent pricing and other real-time control and monitoring. Examples of narrowband PLC systems are specified in international standards such as ITU-T Recommendations G.9902 [2], G.9903 [3] and G.9904 [4], and the IEEE standard 1901.2 [5]. These standards use Orthogonal Frequency Division Multiplexing (OFDM) to deliver scalable data rates up to several hundred kbps over a portion of the European CENELEC band (3–95 kHz in CENELEC-A, 95–125 kHz in CENELEC-B and 125–148.5 kHz in CENELEC-CD) and part of the US FCC band (34.375-487.5 kHz).

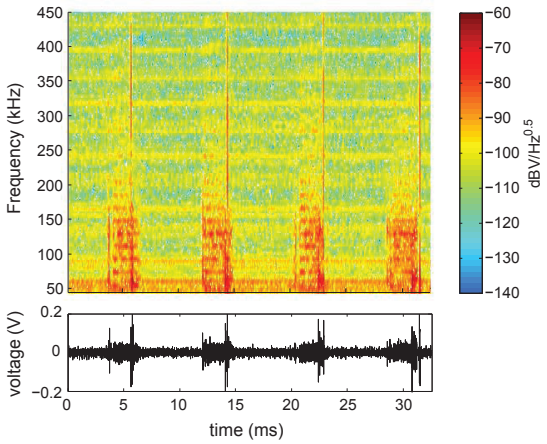

Fig. 1. Spectrogram (top) and time-domain trace (bottom) of an example periodic impulsive noise trace measured from an outdoor low-voltage site [6].

One of the primary challenges for narrowband PLC is to overcome additive powerline noise. Recent field measurements on both indoor and outdoor power lines have identified the dominant noise component in the 3–500 kHz band to be periodic impulsive noise [6], [7], [8], whose statistics varies periodically with half the AC cycle. Such noise exhibits cyclostationarity in both time and frequency domain (Fig.1). In general, it is comprised of two impulsive noise components, whose impulse rates are either synchronous or asynchronous to the main powerline frequency. The synchronous periodic impulsive noise consists of isolated impulses with a repetition rate equal to twice the main powerline frequency. These high-amplitude wideband impulses are typically caused by nonlinear power electronic devices, such as silicon controlled rectifiers and diodes, that switch on and off with the AC cycle while generating abrupt switching transients. On the other hand, the asynchronous periodic impulsive noise takes the form of bursts that occur twice per AC cycle. Each burst consists of an impulse train whose impulse rates are unrelated to and much higher than the main powerline frequency. The

This work was supported by gift funding and equipment donations from National Instruments, as well as grant funding from the Semiconductor Research Corporation under Task ID 1836.133 with liaisons Freescale Semiconductor and Texas Instruments. Part of the work was presented in the 2015 IEEE International Conference on Communications.

J. Lin (jslin@qti.qualcomm.com) is currently with Qualcomm Technologies, Inc., Santa Clara, CA 95051 USA.

J. Lin and B. L. Evans (bevans@ece.utexas.edu) performed this research at the Wireless Networking and Communications Group, The University of Texas at Austin, Austin, TX 78712 USA.

T. Pande (t-pande@ti.com), I. H. Kim (il-han-kim@ti.com) and A. Batra (batra@ieee.org) are with Texas Instruments, Inc., Dallas, TX 75243 USA.

periodic structure within each impulse train results in a sparse power spectral density where the noise power is concentrated around a few frequency components, similarly to that of narrowband interference. A primary contributor to the asynchronous periodic impulsive noise is switching mode power supplies, such as inverters and DC-DC converters, which contain MOSFET switches operating at frequencies above 20 kHz and up to several hundred kHz. These circuits output inband harmonic contents that cannot be perfectly removed by analog filtering.

In addition to the periodic impulsive noise, PLC systems within a smart grid network also suffer from uncoordinated interference from neighboring PLC devices. Such interference is generally characterized by asynchronous impulsive noise [9], which consists of high amplitude impulses that occur randomly in time. The uncoordinated interference can be reduced using multiple access protocols. It can also be mitigated at the receiver using various pre-processing methods [10]. In this work, we focus on combating periodic impulsive noise, and assume that the uncoordinated interference has either been avoided by perfect scheduling all PLC transmissions within a network, or been removed by receiver pre-processing.

Compared to single-carrier communication systems, OFDM is known to be more resilient to frequency-selective channel. Therefore, it can be expected that OFDM also provides inherent immunity to periodic impulsive noise, due to its frequency-selective power spectral density. However, conventional OFDM systems might still encounter dramatic performance degradation in periodic impulsive noise since the noise level in a portion of the transmission band might reach 30–50 dB higher than the background noise, resulting in low SNR in corresponding subcarriers.

To compensate for the performance loss, current narrowband PLC standards adopt concatenated forward error correction coding combined with frequency-domain block interleaving [2], [3], [4], [5], at the expense of reduced throughput and increased implementation complexity. On the receiver side, pre-processing algorithms exploiting the cyclostationarity [11], [12], [13] and time-domain sparsity [10] of the periodic impulsive noise were derived for noise mitigation. These methods, however, demonstrated limited performance gains [11], [12], [13], or required time-domain block interleaving that is not supported by current narrowband PLC standards [10].

In this paper, we aim at improving reliability of OFDM-based narrowband PLC systems in periodic impulsive noise without reducing throughput. Towards that end, we adopt modulation diversity [14], [15] and propose a time-frequency modulation diversity technique that exploits the channel diversity provided by the periodically varying and spectrally shaped noise. An attractive feature of modulation diversity, compared to other diversity schemes, is that it does not incur data rate reduction or bandwidth expansion [14]. More specifically, instead of transmitting individual data symbols, modulation diversity jointly modulates multiple symbols using higher dimensional signal constellations, and transmits components of each signal point over different sub-channels. The modulation itself does not change the data rate in bits per sub-channel.

To improve the robustness of the diversity combining receiver, we propose a semi-online noise power spectrum estimation algorithm that is able to iteratively infer noise power spectrums from received signal, while partially relying on noise measurements prior to transmission. The noise power spectrum is estimated by sparse Bayesian learning techniques, which exploits the redundancy in the cyclic prefix of OFDM symbols, and the frequency-domain sparsity of the asynchronous periodic impulsive noise.

The proposed transceiver methods and conducted simulations are established primarily on the following assumptions. As mentioned previously, we assume that uncoordinated interference (if any) has been avoided or removed by existing techniques. To characterize various statistical properties of periodic impulsive noise, we adopt the linear periodically time varying noise model as specified in the IEEE 1901.2 narrowband PLC standard. A detailed discussion of the noise model is provided in Section II-A. In addition, to design the time-frequency modulation diversity scheme, it is assumed that the receiver is able to make some noise measurements prior to transmission and notify the transmitter, via a feedback link, about the burst duration within each period of the noise. Furthermore, we assume that duration of a transmitted packet is longer than that of a single noise burst. When the packet duration is shorter than a noise burst, joint processing over multiple packets might be desired, which will be deferred to future work due to space constraint.

The rest of the paper is organized as follows. We start in Section II with a description of statistical models for periodic impulsive noise in narrowband PLC, which will be used for emulating the noise in our simulations. We then give a detailed overview of existing transmitter and receiver methods for combating periodic impulsive noise or noise that has similar statistical properties (e.g. cyclostationarity, sparsity, etc.). We introduce time-frequency modulation diversity in Section III, and the diversity receiver for non-coherent and coherent systems in Section IV. In Section V, we present various alternatives for noise power spectrum estimation, focusing on the proposed semi-online algorithm based on sparse Bayesian learning. Finally, the communication performance and implementation complexity of the proposed transceiver methods are evaluated in Section VI.

II. Prior Work

In this section, we briefly review related work on modeling and combating periodic impulsive noise in narrowband PLC.

A. Statistical Models of Periodic Impulsive Noise

Several statistical models have been suggested in the literature to capture the temporal and spectral properties of the periodic impulsive noise. In [7], the noise was expressed as a cyclostationary Gaussian process whose instantaneous variance is a periodic function of time. A linear time invariant filter was used for shaping the noise spectrum. This model, however, is unable to capture the variation of noise power spectral density over time.

A more general linear periodically time varying (LPTV) system model was proposed in [6] and later adopted by

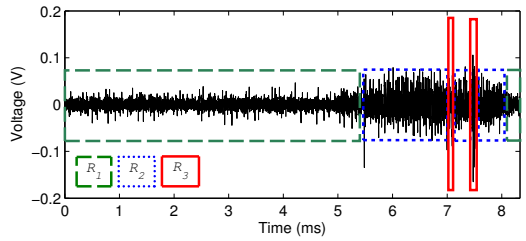

Fig. 2. One period of the exemplified noise in Fig.1 can be partitioned into three intervals $\{\mathcal{R}_i\}_{i=1}^3$. Within each interval the noise is a stationary Gaussian process.

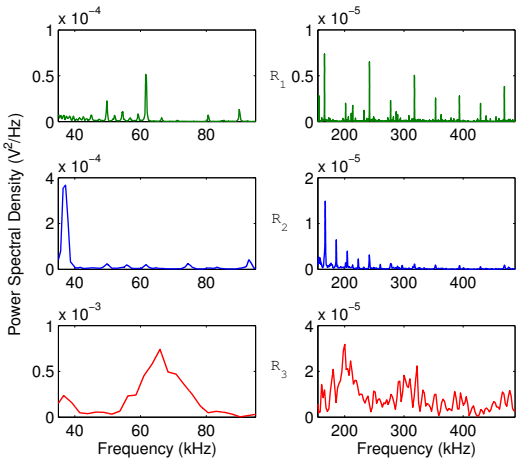

Fig. 3. Power spectral density in the CENELEC-A (left) and FCC (right) bands for the exemplified noise in three stationary intervals $\{\mathcal{R}_i\}_{i=1}^3$.

the IEEE 1901.2 narrowband PLC standard. The model was established on the approximation that each period of the noise can be partitioned into a number of intervals, and that within each interval the noise is a stationary Gaussian process characterized by a particular power spectral density. For example, the noise trace in Fig. 1 can be modeled as a cyclostationary Gaussian process where each period consists of three stationary intervals $\{\mathcal{R}_i\}_{i=1}^3$ (Fig. 2). The third stationary interval is comprised of wideband impulsive noise synchronous to the main powerline frequency. The first two contain periodic impulsive noise asynchronous to the main powerline frequency, which can be identified from the sparse power spectral densities (Fig. 3).

Using the LPTV system model, we can emulate periodic impulsive noise in Fig. 1 by passing additive white Gaussian noise (AWGN) through three linear time invariance filters, and switching the output periodically among them. The frequency response of each filter is fitted to the measured noise power spectral density in the corresponding stationary interval.

B. Existing Transmitter and Receiver Methods

Prior work on combating periodic impulsive noise in OFDM systems involves efforts from both the transmitter and receiver's perspectives. Transmitters specified in existing narrowband PLC standards rely on forward error correction coding and frequency-domain block interleaving to cope with impulsive noise. In particular, it was suggested to use concatenated forward error correction codes (i.e., convolutional, Reed-Solomon and repetition codes) to enhance the error correction capability in harsh channel and noise environments. Heavy coding, however, sacrifices throughput (or equivalently, requires bandwidth expansion) for improved reliability. Most narrowband PLC standards adopt frequency-domain interleaving, i.e., bit-level interleaving prior to the inverse Fast Fourier Transform (IFFT). Sample-level time-domain and time-frequency-domain interleaving were proposed in [16], [17] due to their superior performance over frequency-domain interleaving at high SNRs. However, in order to store the continuous-valued time-domain signal, these interleavers require considerably larger memory than the bit-level frequency-domain interleavers, while the performance improvement is not as significant at low to moderate SNRs.

On the receiver side, pre-processing methods have been developed to mitigate the impact of periodic impulsive noise. These methods exploited various statistical properties of the noise, according to which they can be divided into two categories. The first type of approach is based on the cyclostationary noise model [6]. These methods parameterized the second-order noise statistics in each stationary interval by either a correlation matrix [18] or filter coefficients [11], [12], [13], and estimated the parameters by training. Based on the estimated parameters, equalizers [18], [13] or prediction filters [11], [12] were designed to essentially transform the spectrally shaped noise into AWGN. These parametric approaches are sensitive to parameter estimation errors. Accurate parameter estimation generally requires large training overhead and a huge memory that might not exist at narrowband PLC receivers.

A second class of receiver methods utilizes sparsity of the noise in time domain to estimate and subtract the noise bursts and impulses from received signal. These methods observe the impulsive noise on various subcarriers of the received OFDM symbols, and apply compressed sensing techniques to recover the noise impulses [19], [10]. In particular, our recent study [10] targeting periodic impulsive noise in narrowband PLC adopted time-domain block interleaving [16] to spread the noise bursts into short impulses over multiple OFDM symbols, and estimated the impulses by sparse Bayesian learning [20].

Compared to previous studies, our proposed joint transmitter-receiver design has several advantages. Unlike concatenated forward error correction coding, our transmission scheme using modulation diversity does not decrease data rates for improved robustness. Secondly, the whole transceiver design can be easily integrated into existing narrowband PLC standards. In particular, it does not depend on time-domain interleaving, which is an essential element in [10], [16], [17] but is not standard-compliant. Our proposed transceiver methods also bring significant memory savings compared to [10], [16], [17], thanks to the use of frequency-domain interleaving. Lastly, the proposed semi-online noise power estimator is primarily data-driven, and therefore saves significant training overhead compared to the parametric noise mitigation methods [11], [12], [13], [18].

TABLE I
OPTIMAL PARAMETERS FOR THE LENGTH-N_d HOCHWALD/SWELDENS CODE IN $i.i.d.$ FLAT RAYLEIGH FADING AND AWGN [22].

N_d	2	3	4
$[u_1 \cdots u_{N_d}]$	[1 1]	[1 1 3]	[1 3 5 7]

III. TIME-FREQUENCY MODULATION DIVERSITY

In general, modulation diversity refers to modulation schemes that jointly map a number of bits to a multi-dimensional constellation point ($a.k.a.$ a codeword), the components of which are transmitted over different sub-channels. The goal is to improve communication reliability by spreading information over multiple sub-channels and hence exploiting channel diversity.

Several categories of modulation diversity codes have been investigated in the literature [14], [21], among which the Hochwald/Sweldens codes have attracted a lot of attention [15], [22]. A Hochwald/Sweldens codebook defines a one-to-one mapping from any group of N_dR bits to an N_d dimensional constellation point, each dimension of which is a phase shift keying (PSK) symbol:

$$f : \mathbf{c} \in \{0,1\}^{N_dR} \rightarrow \mathbf{s} \in \mathcal{C}^{N_d}. \tag{1}$$

Here R denotes the original data rate in bits per symbol, and $\mathcal{C}$ denotes a 2^{N_dR}-PSK constellation. Note that the same data rate of R is maintained after modulation diversity, if the N_d components of $\mathbf{s}$ are transmitted over different sub-channels. The n-th component of a codeword $\mathbf{s}^{(m)}$ has the form

$$s_n^{(m)} = \exp(j2\pi u_n m/2^{N_dR}), \tag{2}$$

$\forall m = 1, \cdots, 2^{N_dR}$, $\forall n = 1, \cdots, N_d$. When $u_n = 1, \forall n$, the Hochwald/Sweldens code reduces to a PSK repetition code [14]. In general, $\mathbf{u} \triangleq [u_1 \cdots u_{N_d}]$ need to be optimized to minimize the symbol error rate in specific channel conditions. Assuming that all components of a codeword are transmitted over static flat channels or $i.i.d.$ flat Rayleigh fading channels and corrupted by AWGN, the optimal values of $\mathbf{u}$ for $R = 1$ and $N_d = 2$ to 4 have been found by exhaustive search [22] and are summarized in Table III.

Modulation diversity has been applied in various forms and demonstrated superior communication performance in multi-antenna communications [15] and in OFDM systems [23]. In [15], a unitary space-time modulation scheme was derived based on the Hochwald/Sweldens codes. In [23], dual carrier modulation was proposed to exploit channel diversity in frequency domain in ultra-wideband wireless communications.

In OFDM-based narrowband PLC systems, recognizing the periodically varying spectrally shaped statistics of periodic impulsive noise, we propose to apply modulation diversity across time and frequency, which leads to the time-frequency modulation diversity (TFMD). In TFMD, components of a modulation diversity codeword are transmitted on various subcarriers in multiple OFDM symbols. To achieve better performance, such time-frequency mapping needs to be configured properly according to the burst structure of the noise and the OFDM parameters. A simple mapping scheme is depicted in Fig. 4, assuming $N_d = 2$ as an example. In general, the N_d components of a modulation diversity codeword are spread into time and frequency units so that adjacent components are separated by ΔK subcarriers and ΔT OFDM symbols. To reduce the possibility that all components are affected by narrowband interference or a deep fade in frequency domain, we divide the transmission band evenly into N_d subbands, and distribute the components in different subbands, i.e., $\Delta K = N_{\text{data}}/N_d$, where N_{data} denotes the number of data subcarriers in an OFDM symbol. Likewise, to ensure that not every component of a codeword is contaminated by noise bursts, ΔT is set to be the maximum number of consecutive OFDM symbols in a single noise burst. Thanks to the cyclostationary property of the noise, the burst duration within a period of the noise can be pre-determined by the receiver and made available to the transmitter via receiver feedback.

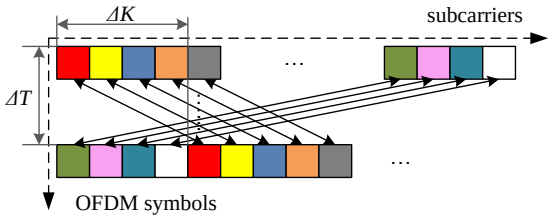

Fig. 4. An example of time-frequency modulation diversity. The two components of a codeword (marked in the same color) are allocated to subcarriers i in OFDM symbol j, and subcarrier $\big((i+\Delta K) \mod N_{\text{data}}\big)$ in OFDM symbol $\big((j+\Delta T) \mod N_{\text{OFDM}}\big)$, $\forall i, j$, where N_{data} is the number of data subcarriers in an OFDM symbol, and N_{OFDM} is the number of OFDM symbols in a packet.

We adopt a Hochwald/Sweldens codebook since it produces PSK symbols. PSK is a mandatory modulation scheme in the ITU-T G.9903, G.9904 and the IEEE 1901.2 narrowband PLC standards. Ideally, the parameters $\mathbf{u}$ need to be optimized taking into account the PLC channel models. In particular, amplitude of PLC channels is typically characterized by log-normal distributions rather than Rayleigh fading [24]. Furthermore, for a given PLC link, the channel frequency response is fairly static and can be determined from the topology and impedance properties of the cable [25]. Since this paper is focused on combating periodic impulsive noise, we leave the design of optimal codebooks based on PLC channel models for future work. The receiver methods presented in the following can be applied to arbitrary $\mathbf{u}$.

The block diagram for an OFDM-based narrowband PLC transmitter using TFMD is shown in Fig. 5 and compared with a conventional transmitter operating in DBPSK/BPSK mode, using similar physical layer specifications as in the ITU-T G.9903 standard. In the conventional transmitter, the binary data is protected by an optional Reed-Solomon code, a convolutional code and an interleaver with scalable depths up to an entire packet. The interleaved bits are modulated into BPSK symbols, which are then allocated to the data tones of the OFDM symbols. The transmitter can be configured to operate in either of the two transmission modes: non-coherent (i.e., differential) and coherent. In a non-coherent system, a reference OFDM symbol is inserted at the beginning of a packet, upon which the following symbols are differentially encoded in the time domain, i.e., each subcarrier is differentially encoded based on the same subcarrier in the

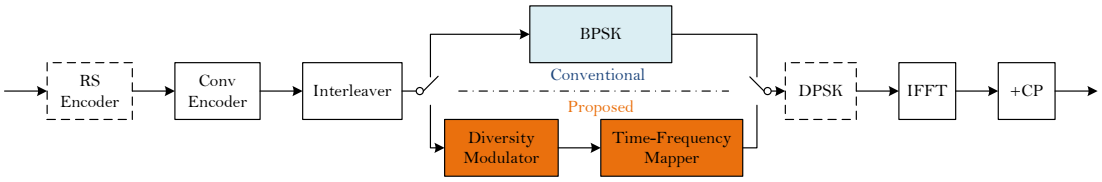

Fig. 5. The block diagram of a conventional OFDM-based narrowband PLC transmitter using BPSK modulation, compared to the proposed transmitter using time-frequency modulation diversity. The time-frequency mapper allocates components of every Hochwald/Sweldens codeword to different subcarriers in various OFDM symbols. The dashed blocks, i.e., the Reed-Solomon (RS) encoder and differential encoder (DPSK), can be optionally switched on and off.

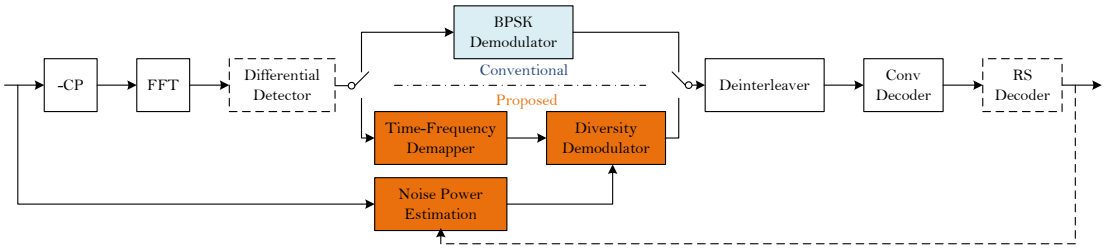

Fig. 6. The block diagram of a conventional OFDM-based narrowband PLC receiver, compared to the proposed diversity receiver. The differential detector can be switched on (in non-coherent mode) or off (in coherent mode). The time-frequency demapper groups signals received on different sub-channels in different OFDM symbols, which are combined by the diversity demodulator based on the estimated noise power spectrums. In non-coherent mode, the noise power spectrums can be estimated before transmission. In coherent mode, it can also be estimated iteratively using a semi-online method, using decision feedback from the decoder. The dashed blocks, i.e., the Reed-Solomon (RS) decoder and differential detector, can be optionally switched on and off.

previous symbol. In a coherent system, each OFDM symbol contains multiple pilot tones for channel estimation. In both transmission schemes, the OFDM symbols are passed through an inverse Fast Fourier Transform (IFFT), after which a cyclic prefix (CP) is inserted at the beginning of each symbol to prevent inter-symbol interference. Our proposed transmitter is built upon the conventional transmitter, by replacing the BPSK modulator with the TFMD modulator. More specifically, the TFMD modulator is comprised of a diversity modulator that maps every N_d bits to N_d PSK symbols, and a time-frequency mapper that allocates the PSK symbols to N_d designated time-frequency units. Note that the data rates (in bits per sub-channel) are the same before and after modulation.

IV. Soft-Output Diversity Demodulation

Given the transmitter structure in Fig. 5, a diversity demodulator combines received signal in N_d time-frequency slots to generate soft decisions on the N_d bits. Such combining depends on the estimation of the periodically varying noise power spectral density.

Let us first consider the non-coherent transmission scheme. We have a group of bits, $\mathbf{c} \in \{0,1\}^{N_d}$, that is jointly mapped to a modulation diversity codeword. Suppose that the n-th component of the codeword is allocated to subcarrier i_n in the j_n-th OFDM symbol, $\forall n = 1, \cdots, N_d$, which is denoted by $v_{i_n j_n}$. To simplify notations, define index sets $I \triangleq \{i_n\}_{n=1}^{N_d}$ and $J \triangleq \{j_n\}_{n=1}^{N_d}$, and a column vector $\mathbf{v}_{IJ} \triangleq \{v_{i_n j_n}\}_{n=1}^{N_d}$. The OFDM symbols are differentially encoded in the time domain, which results in

$$\mathbf{s}_{IJ} = \mathbf{v}_{IJ} \odot \mathbf{s}_{I,J-1},$$

where $\mathbf{s}_{I,J-1} \triangleq \{s_{i_n,j_n-1}\}_{n=1}^{N_d}$, and $\odot$ denotes the pointwise product between two vectors.

One of the most important properties of OFDM is that it divides a frequency-selective channel to multiple narrowband flat sub-channels, each of which is centered at a subcarrier frequency. Assuming that the CP is longer than the channel delay spread, the receiver discards the CP and takes an FFT of the rest of the OFDM symbol, which leads to

$$\mathbf{r}_{IJ} = \mathbf{h}_{IJ} \odot \mathbf{s}_{IJ} + \mathbf{e}_{IJ}.$$

Here $h_{i_n j_n}$ denotes the complex amplitude of the sub-channel, and $e_{i_n j_n}$ is the additive noise.

The soft decisions on $\mathbf{c}$ consists of N_d log-likelihood ratios (LLRs), one for each bit. Each of the LLRs is conditioned on the received signal $\mathbf{r}_{IJ}$ and the reference signal $\mathbf{r}_{I,J-1}$:

$$\begin{aligned} L(c_n) &= \ln \frac{p(c_n = 0 | \mathbf{r}_{IJ}, \mathbf{r}_{I,J-1})}{p(c_n = 1 | \mathbf{r}_{IJ}, \mathbf{r}_{I,J-1})} \\ &\approx \ln \frac{\max\limits_{\mathbf{v}_{IJ}: c_n = 0} p(\mathbf{r}_{IJ} | \mathbf{v}_{IJ}, \mathbf{r}_{I,J-1})}{\max\limits_{\mathbf{v}_{IJ}: c_n = 1} p(\mathbf{r}_{IJ} | \mathbf{v}_{IJ}, \mathbf{r}_{I,J-1})}. \end{aligned} \quad (3)$$

In (3), the max-sum approximation of the exact LLR is applied to reduce the computational complexity as in [26]. Assuming that the additive noise samples on different subcarriers are mutually uncorrelated, the likelihood expressions in (3) can be derived following standard routines similarly as in [27]

$$p(\mathbf{r}_{IJ} | \mathbf{v}_{IJ}, \mathbf{r}_{I-1,J}) = \mathcal{CN}(\mathbf{r}_{I,J-1} \odot \mathbf{v}_{IJ}, \tilde{\boldsymbol{\sigma}}_{IJ}), \quad (4)$$

where $\tilde{\boldsymbol{\sigma}}_{IJ} = \boldsymbol{\sigma}_{I,J-1} + \boldsymbol{\sigma}_{IJ}$, and $\sigma_{i_n j_n}$ is the noise variance in the corresponding time-frequency slot, i.e., $\sigma_{i_n j_n} \triangleq \mathbb{E}[|e_{i_n j_n}|^2], \forall n$. Substituting (4) into (3) results in

$$\begin{aligned} L(c_n) &= \max_{\mathbf{v}_{IJ}: c_n = 0} \sum_{k=1}^{N_d} \frac{\mathrm{Re}\{r_{i_k j_k} v_{i_k j_k}^* r_{i_k, j_k - 1}^*\}}{\tilde{\sigma}_{i_k j_k}} - \\ &\quad \max_{\mathbf{v}_{IJ}: c_n = 1} \sum_{k=1}^{N_d} \frac{\mathrm{Re}\{r_{i_k j_k} v_{i_k j_k}^* r_{i_k, j_k - 1}^*\}}{\tilde{\sigma}_{i_k j_k}}. \end{aligned} \quad (5)$$

Compared to conventional DPSK detection [27], the diversity demodulator (5) combines the decision metrics from N_d time-frequency slots, with the weights inversely proportional to the noise variances.

In addition to using a two-symbol observation window for differential detection, the diversity demodulator can also be generalized to use multiple-symbol differential detection, given that increasing the window size generally leads to better performance [26], [27], [28]. The generalized diversity demodulator computes LLRs conditioned on $\{\mathbf{r}_{IJ}, \mathbf{r}_{I,J-1}, \cdots, \mathbf{r}_{I,J-N_w+1}\}$, where N_w is the window size. However, multiple-symbol differential detection requires much higher implementation complexity, and hence might be infeasible for low-power low-cost PLC systems. As such, throughout the rest of the paper, we will only use two-symbol observation windows for differential detection.

Following similar derivations, it can be verified that the diversity demodulator for coherent systems take the same mathematical form as (5), except for replacing the reference signal r_{i_k,j_k-1} with the channel estimation $\hat{h}_{i_kj_k}$, and $\tilde{\sigma}_{i_kj_k}$ with $\sigma_{i_kj_k}$. Fig. 6 depicts the modulation diversity receiver that takes into account of the cyclostationary noise statistics, compared with a conventional OFDM receiver assuming AWGN.

V. Noise Power Estimation

The gain of diversity combining depends on the accuracy of noise power estimation. In this section, we first discuss an offline estimator that measures noise power spectrums prior to transmission. Such offline approach can be applied to both non-coherent and coherent systems. After that, we will show that in coherent systems, a semi-online algorithm can be derived to iteratively infer noise power spectrums from the received signal, based on certain coarse measurements obtained prior to transmission.

In the offline approach, the receiver collects noise samples that span multiple AC cycles before the transmission starts, and uses that to estimate noise power spectrums. More specifically, it takes a short time Fourier transform (by sliding FFT) over the recorded noise samples, and averages the instantaneous noise power spectrums in each stationary interval.

Generally, such offline estimation becomes more accurate as more noise samples are collected. Consider a single PLC link, it appears that the idle interval between consecutive transmissions typically takes several minutes, covering thousands of AC cycles. For example, a smart meter reports customer load profile to a data concentrator every 15 minutes [29]. However, within a smart grid network, PLC transmissions from different devices need to be scheduled using multiple access protocols (e.g. carrier sense multiple access) to limit uncoordinated interference [30]. As the number of PLC devices increases, the length of idle intervals, when none of the devices is transmitting, becomes limited. In this situation, a receiver might not be able to collect sufficient noise samples to make accurate noise power estimation, or more advanced techniques have to be used to discriminate powerline noise from transmissions by neighboring devices. Therefore, it is desirable to develop algorithms to estimate noise power spectrums primarily during data transmission.

Towards that end, we notice that the stationary intervals can be divided into two categories. The type-1 stationary intervals contains periodic impulsive noise asynchronous to the main powerline frequency, and is characterized by a sparse power spectral density (e.g. $\mathcal{R}_1$ and $\mathcal{R}_2$ in the examplified noise trace in Fig. 2). The type-2 stationary intervals consists of wideband impulsive noise whose power spectral density reaches much higher than that in the rest of the period (e.g. $\mathcal{R}_3$ in Fig. 2). Since the entire band is overwhelmed by high power noise in the type-2 stationary intervals, according to (5), signal received therein is supposed to be lightly weighted in the diversity combining, and therefore is generally negligible without causing noticeable performance degradation. In the following, we present a semi-online algorithm that estimates the noise power spectrums in the type-1 stationary intervals by exploiting its sparsity structure.

A. Problem Formulation

Let N_c and N_p denote the FFT size and CP length in an OFDM system, and L_h the channel delay spread in samples. Most narrowband PLC standards adopt a CP that is much longer than typical channel delay spreads (i.e., $N_p \gg L_h$). For example, the root-mean-square delay spreads encountered in the narrowband PLC field measurements are $2-6\mu s$ [9], whereas the CP durations specified by the ITU-T G.9903 standard are $75\mu s$ in the CELENEC-A band (at the sampling frequency of 400 kHz), and $25\mu s$ in the FCC band (at the sampling frequency of 1.2 MHz) [3]. The first L_h samples inside the CP are affected by inter-symbol-interference. Removing these samples from the j-th received OFDM symbol in time domain results in

$$\dot{\mathbf{r}}_j = \mathbf{H}_j \mathbf{S} \mathbf{F}_{N_c}^* \mathbf{s}_j + \dot{\mathbf{e}}_j.$$

Here $\mathbf{F}_{N_c}$ is the N_c-point FFT matrix, $\mathbf{S} \triangleq \begin{bmatrix} \mathbf{0}_{N_c-N_p+L_h} & & \mathbf{I}_{N_p-L_h} \\ & \mathbf{I}_{N_c} & \end{bmatrix}$, $\mathbf{H}_j$ is a Toeplitz matrix consisting of a time shifted channel impulse response in each row, $\dot{\mathbf{r}}_j$ and $\dot{\mathbf{e}}_j$ denote the time-domain received signal and additive noise, respectively.

Define a matrix $\mathbf{W}$ as

$$\mathbf{W} \triangleq \begin{bmatrix} \mathbf{A} & \mathbf{0}_{(N_p-L_h)\times(N_c-N_p+L_h)} & -\mathbf{A} \end{bmatrix},$$

where $\mathbf{A}$ is an arbitrary $(N_p-L_h)\times(N_p-L_h)$ unitary matrix. It can be easily proved that $\mathbf{W}\mathbf{H}_j\mathbf{S} = \mathbf{0}, \forall \mathbf{A}$, as long as $\mathbf{H}_j$ is Toeplitz. Therefore pre-multiplying $\dot{\mathbf{r}}_j$ by $\mathbf{W}$ removes the information bearing portion from the CP, i.e.,

$$\mathbf{y}_j \triangleq \mathbf{W}\dot{\mathbf{r}}_j = \mathbf{W}\dot{\mathbf{e}}_j. \tag{6}$$

We assume no uncoordinated interference, so that the additive noise $\dot{\mathbf{e}}_j$ is dominated by periodic impulsive noise. As mentioned previously in Section I, the periodic impulsive noise asynchronous to the main powerline frequency has a sparse power spectral density (Fig. 3). This type of noise can therefore be decomposed in the frequency domain as

$$\dot{\mathbf{e}}_j = \mathbf{F}_N^*(\mathbf{x}_j + \mathbf{g}_j),$$

where $N = N_c + N_p - L_h$, $\mathbf{x}_j$ is a sparse vector, $\mathbf{g}_j$ captures the residual background noise and is approximated

by AWGN. Defining $\mathbf{\Phi} \triangleq \mathbf{W}\mathbf{F}_N^*$ and $\mathbf{v}_j \triangleq \mathbf{W}\mathbf{F}_N^*\mathbf{g}_j$, (6) can be succinctly rewritten as

$$\mathbf{y}_j = \mathbf{\Phi}\mathbf{x}_j + \mathbf{v}_j. \tag{7}$$

Note that $\mathbf{v}_j$ is still AWGN since $\mathbf{A}$ and $\mathbf{F}_N$ are both unitary.

Suppose that before the transmission starts, the receiver has collected a few periods of noise samples using the idle intervals. it can roughly determine how to partition one period of the noise into multiple stationary intervals. Based on that information, the receiver is able to identify the OFDM symbols that are received during each of the type-1 stationary intervals. We thereby group the corresponding measurement vectors $\mathbf{y}_j$ in the k-th stationary interval, and expand (7) into

$$\mathbf{Y}_k = \mathbf{\Phi}\mathbf{X}_k + \mathbf{V}_k. \tag{8}$$

Here $\mathbf{Y}_k$ is a matrix formed by column vectors $\{\mathbf{y}_j, \forall j \in \mathbb{S}_k\}$, where $\mathbb{S}_k$ is the index set for all OFDM symbols received in the k-th stationary interval. Similar definitions apply to $\mathbf{X}_k$ and $\mathbf{V}_k$. Note that all columns of $\mathbf{X}_k$ are sparse vectors that share an identical support. (8) is an example of the standard multiple measurement vector (MMV) problem in compressed sensing. In the following, we describe an algorithm based on T-MSBL [31] to iteratively estimate the noise power spectrum and decode the received signal, based on (8). The proposed algorithm applies to every type-1 stationary interval, and for conciseness purposes we will omit sub-index k in Section V-B.

B. Noise Power Spectrum Estimation Using T-MSBL

The T-MSBL algorithm uses a sparse Bayesian learning (SBL) approach [20], [32] to solve the generic MMV problem $\mathbf{Y} = \mathbf{\Phi}\mathbf{X} + \mathbf{V}$, where $\mathbf{Y}$ is an $M \times L$ measurement matrix, $\mathbf{\Phi}$ is a known $M \times N$ dictionary matrix, $\mathbf{X}$ is an unknown $N \times L$ source matrix with each row representing a possible source, and $\mathbf{V}$ is an unknown $M \times L$ noise matrix.

The key idea is to exploit the row sparsity of the source matrix $\mathbf{X}$, and impose a sparsity promoting prior on $\mathbf{X}$ that leads to a posterior density that is concentrated over row-sparse matrices. Let $\mathbf{X}_{i\cdot}$ denote the i-th row of $\mathbf{X}$. The algorithm imposes a parameterized Gaussian prior on $\mathbf{X}_{i\cdot}$

$$p(\mathbf{X}_{i\cdot}; \gamma_i, \mathbf{B}) = \mathcal{CN}(\mathbf{X}_{i\cdot}; 0, \gamma_i\mathbf{B}),\ \forall i = 1, \cdots, N \tag{9}$$

where $\boldsymbol{\gamma} \triangleq [\gamma_1\ \cdots\ \gamma_N]$ are nonnegative parameters controlling the row sparsity of $\mathbf{X}$, and $\mathbf{B}$ is a positive definite matrix that captures the covariance of $\mathbf{X}_{i\cdot}$. The maximum a posteriori (MAP) estimation of $\boldsymbol{\gamma}$ and $\mathbf{B}$ can be computed iteratively using the expectation maximization (EM) algorithm. Upon convergence, $\boldsymbol{\gamma}$ will become a sparse vector. To ensure a unique global solution, the number of non-zero rows in $\mathbf{X}$ has to be below a certain threshold.

In our specific problem, when applying the prior (9) to the k-th stationary interval, it is assumed that $\mathbf{x}_j, \forall j \in \mathbb{S}_k$ are temporally correlated, identically distributed Gaussian random vectors. While capturing the temporal correlation, the prior makes an approximation that the frequency components of the noise are uncorrelated with each other, i.e., $\mathbb{E}[\mathbf{x}_j\mathbf{x}_j^*] \triangleq \mathbf{\Gamma}$ is a diagonal matrix. The neglect of frequency-domain correlation significantly reduces the number of parameters to be estimated, and hence prevents overfitting.

A challenge in using T-MSBL to estimate noise power spectrum is that the number of peaks in $\mathbf{x}_j$ generally exceeds the threshold that guarantees a unique global solution. In that case, the EM algorithm may converge to a second global optimum $\boldsymbol{\gamma}^*$ that has a different support than that of the desired global optimum. To better guide the Bayesian inference to converge to the actual noise power spectrum, despite of its low sparsity level, we propose a more informative prior that incorporates decision feedback from the decoder.

On top of the prior (9), we impose a hyper-prior on $\boldsymbol{\gamma}$ and $\mathbf{B}$, respectively. We adopt the following conjugate priors since they generally lead to computationally tractable solutions:

$$p(\boldsymbol{\gamma}; \mathbf{a}, \mathbf{b}) = \prod_{i=1}^{N} \text{IG}(\gamma_i; a_i, b_i), \tag{10}$$

$$p(\mathbf{B}; \mu, \mathbf{\Psi}) = \text{IW}(\mathbf{B}; \mu, \mathbf{\Psi}). \tag{11}$$

Here $\text{IG}(\gamma_i; a_i, b_i)$ is the inverse Gamma distribution with the shape parameter a_i and scale parameter b_i, both of which assume non-negative values; $\text{IW}(\mathbf{B}; \mu, \mathbf{\Psi})$ denotes the inverse Wishart distribution, where $\mu > L$ is the degree of freedom and $\mathbf{\Psi}$ is a positive definite scale matrix.

Upon receiving a packet, the hyperparameters $\mathbf{a}, \mathbf{b}, \mu$ and $\mathbf{\Psi}$ are initialized with non-informative values (e.g. $\mathbf{a} = \mathbf{b} = \mathbf{0}, \mu = L+1, \mathbf{\Psi} = \mathbf{I}_L$), and are then updated iteratively based on decision feedback from the FEC decoder. In each iteration, given the hierarchical prior, the noise power estimator executes a single iteration of the EM algorithm to generate an estimate of $\boldsymbol{\gamma}$. Since $\boldsymbol{\gamma}$ is the N-point noise power spectrum, we need to compute the desired N_c-point noise power spectrum $\boldsymbol{\sigma}$ by

$$\boldsymbol{\sigma} = \text{diag}\Big\{\mathbf{P}\mathbf{\Gamma}\mathbf{P}^*\Big\},$$

where $\mathbf{P} = \mathbf{F}_{N_c}\begin{bmatrix}\mathbf{0}_{N_p - L_h} & \mathbf{I}_{N_c}\end{bmatrix}\mathbf{F}_N^*$, and $\mathbf{\Gamma} \triangleq \text{diag}(\boldsymbol{\gamma})$. The diversity demodulator then combines received signals according to (5), using the current estimate of $\boldsymbol{\sigma}$ for all stationary intervals. The soft outputs, after deinterleaving, are further decoded by the convolutional decoder. In coherent mode, the receiver can use the hard decisions from the decoder (e.g. convolutional or Reed-Solomon decoder) to reconstruct the transmitted signal, which is filtered by the estimated channel, and subtracted from the actual received signal. The residual in the frequency domain, denoted by $\hat{\mathbf{X}}'$, is an estimate of $\mathbf{X}$ and contains side information that is extracted from the redundancy of the convolutional code. Since (10) and (11) are conjugate priors, the posterior distribution of $\boldsymbol{\gamma}$ (or $\mathbf{B}$), conditioned on

$\hat{\mathbf{X}}'$, is also an inverse Gamma (or inverse Wishart) distribution:

$$\begin{aligned} p(\mathbf{B}|\hat{\mathbf{X}}';\mu,\mathbf{\Psi},\boldsymbol{\gamma}) &= \text{IW}(\mathbf{B};\tilde{\mu},\tilde{\mathbf{\Psi}}), \\ \tilde{\mu} &= \mu+N, \\ \tilde{\mathbf{\Psi}} &= \mathbf{\Psi}+\sum_{i=1}^{N}\frac{\hat{\mathbf{X}}_{i\cdot}'^{*}\hat{\mathbf{X}}_{i\cdot}'}{\gamma_i} \qquad (12) \\ p(\boldsymbol{\gamma}|\hat{\mathbf{X}}';\mathbf{a},\mathbf{b},\mathbf{B}) &= \prod_{i=1}^{N}\text{IG}(\gamma_i;\tilde{a}_i,\tilde{b}_i), \\ \tilde{a}_i &= a_i+\frac{L}{2}, \\ \tilde{b}_i &= b_i+\frac{1}{2}\hat{\mathbf{X}}_{i\cdot}'\mathbf{B}\hat{\mathbf{X}}_{i\cdot}'^{*}. \qquad (13) \end{aligned}$$

Note that the side information extracted from the decision feedback $\hat{\mathbf{X}}'$ is fused into the updated hyperparameters $\tilde{\mathbf{a}},\tilde{\mathbf{b}},\tilde{\mu}$, and $\tilde{\mathbf{\Psi}}$. These more informative hyper-priors are then used for noise power spectrum estimation in the next iteration. As such, we formulate a receiver that iteratively estimates noise power spectrums in all type-1 stationary intervals using decision feedback from the decoder, and uses the estimation to decode the received signal. Multiple iterations are run for every single packet. To reduce error propagation, the noise power estimation from one packet does not carry over to the next packet, i.e., the hyperparameters are re-initialized for every received packet. The iterative receiver structure described above is depicted in Fig. 6. Such receiver can be applied in coherent mode only, since it requires channel estimation to reconstruct the received signal from the decoder output.

Given the hierarchical prior, the MAP estimation of $\boldsymbol{\gamma}$ and $\mathbf{B}$ can be computed iteratively using the EM algorithm, following similar routines as in [31]. We summarize the T-MSBL algorithm with the hierarchical prior in Algorithm 1, while deferring the derivation details to the Appendix. Compared to the standard T-MSBL algorithm in [31], the update rules for $\boldsymbol{\gamma}$ and $\mathbf{B}$ now involves additional hyperparameters $\mathbf{a},\mathbf{b},\mu$ and $\mathbf{\Psi}$, which provide extra information on $\mathbf{X}$. Note again that the algorithm needs to be applied to all type-1 stationary intervals.

Algorithm 1 T-MSBL with Hierarchical Prior

1: Initialization:

$$\begin{aligned} &\boldsymbol{\gamma}^{(0)}=\mathbf{1},\mathbf{B}^{(0)}=\mathbf{I}_L,\lambda^{(0)}=0, \\ &\mathbf{a}^{(0)}=\mathbf{0},\mathbf{b}^{(0)}=\mathbf{0},\mu^{(0)}=L+1,\mathbf{\Psi}^{(0)}=\mathbf{I}_L \end{aligned}$$

2: **for** $t=1,\cdots,T$ **do**

3: E-Step:

$$\begin{aligned} \mathbf{\Xi}^{(t)} &= \Big((\mathbf{\Gamma}^{(t)})^{-1}+\frac{1}{\lambda^{(t)}}\mathbf{\Phi}^{*}\mathbf{\Phi}\Big)^{-1}, \\ \hat{\mathbf{X}}^{(t)} &= \mathbf{\Gamma}^{(\mathbf{t})}\mathbf{\Phi}^{*}(\lambda^{(t)}\mathbf{I}_L+\mathbf{\Phi}\mathbf{\Gamma}^{(\mathbf{t})}\mathbf{\Phi}^{*})^{-1}\mathbf{Y}. \end{aligned}$$

4: M-Step:

$$\begin{aligned} \gamma_i^{(t+1)} &= \frac{\hat{\mathbf{X}}_{i\cdot}^{(t)}(\mathbf{B}^{(t)})^{-1}\hat{\mathbf{X}}_{i\cdot}^{(t)*}+L\mathbf{\Xi}_{ii}^{(t)}+2b_i^{(t)}}{L+2a_i^{(t)}}, \\ &\quad \forall i=1,\cdots,N, \qquad (14) \\ \tilde{\mathbf{B}}^{(t+1)} &= \sum_{i=1}^{N}\frac{\hat{\mathbf{X}}_{i\cdot}^{(t)*}\hat{\mathbf{X}}_{i\cdot}^{(t)}}{\gamma_i^{(t)}}+\mathbf{\Psi}^{(t)*}, \qquad (15) \\ \mathbf{B}^{(t+1)} &= \tilde{\mathbf{B}}^{(t+1)}/||\tilde{\mathbf{B}}^{(t+1)}||_{\mathcal{F}}, \\ \lambda^{(t+1)} &= \frac{1}{ML}||\mathbf{Y}-\mathbf{\Phi}\hat{\mathbf{X}}^{(t)}||_{\mathcal{F}}^{2}+ \\ &\quad \frac{\lambda^{(t)}}{M}\text{Tr}\big[\mathbf{\Phi}\mathbf{\Gamma}^{(t)}\mathbf{\Phi}^{*}\big(\lambda^{(t)}\mathbf{I}_M+\mathbf{\Phi}\mathbf{\Gamma}^{(t)}\mathbf{\Phi}^{*}\big)^{-1}\big]. \end{aligned}$$

5: Update hyperparameters using decision feedback:

$$\begin{aligned} a_i^{(t+1)} &= a_i^{(t)}+L/2,\forall i=1,\cdots,N, \\ b_i^{(t+1)} &= b_i^{(t)}+\frac{1}{2}\hat{\mathbf{X}}_{i\cdot}'^{(t)}\mathbf{B}^{(t+1)}\hat{\mathbf{X}}_{i\cdot}'^{*(t)},\forall i=1,\cdots,N, \\ \mu^{(t+1)} &= \mu^{(t)}+N, \\ \mathbf{\Psi}^{(t+1)} &= \mathbf{\Psi}^{(t)}+\sum_{i=1}^{N}\frac{\hat{\mathbf{X}}_{i\cdot}'^{*(t)}\hat{\mathbf{X}}_{i\cdot}'^{(t)}}{\gamma_i}. \end{aligned}$$

6: **end for**

VI. Communication Performance and Implementation Complexity

In this section, we evaluate communication performance and implementation complexity of the proposed transceiver methods in periodic impulsive noise. The evaluation is in comparison to a reference OFDM-based narrowband PLC system as suggested by the ITU-T G.9903 standard.

A. Communication Performance

To evaluate the bit error rate (BER) performance in periodic impulsive noise, we inject both realistic and synthetic noise into the transmit signal. The realistic noise was measured from an outdoor low-voltage power line in [6]. A segment of the time-domain noise trace has been shown in Fig. 1. The synthetic noise is generated using the LPTV system model as described in Section II-A. More specifically, we partition each period of the noise into three stationary intervals, which covers $70\%, 29\%$ and 1% of a period, respectively. In each stationary interval, the noise is spectrally shaped using the power spectral density profile from the same field measurement in [6], which is also available in the IEEE 1901.2 standard [5]. The BER statistics is averaged over 10^4 data packets. In synthetic noise, each packet has an independent noise realization. For simplicity, we assume flat channel throughout the simulations.

We simulate the physical layer of the proposed TFMD transceiver and a reference narrowband PLC system, both of which adopt standard parameters as specified in the ITU-

TABLE II
Physical layer parameters of the reference and proposed narrowband PLC systems.

Parameters	CENELEC-A		FCC	
	Reference	TFMD	Reference	TFMD
Sampling Frequency	400 kHz		1.2 MHz	
FFT Size N_c	256			
CP Length N_p	30			
# of Subcarriers	128			
Data Subcarriers	23–58		33–104	
Convolutional Code	rate 1/2, length 7			
Reed-Solomon Code	251/235	N/A	125/109	N/A
Interleaver Size (Bits)	4032	36	2016	72
Packet Size (Bytes)	235		109	
Data Rate (kbps)	23.5	25	130.7	146.4

T G.9903 Recommendations (Table II). Both systems can be configured to operate in either non-coherent or coherent modes, and transmit in one of the two bands: 35.9–90.6 kHz in the CENELEC-A band and 154.7–487.5 kHz in the FCC band. In non-coherent mode, a reference OFDM symbol is inserted at the beginning of each packet for differential encoding; whereas in coherent mode, for simplicity purposes we do not insert any pilots for channel estimation, since a flat channel is assumed in the simulations. As suggested by the standard, the reference system uses concatenated Reed-Solomon and convolutional coding, whole-packet interleaving, and DBPSK/BPSK modulation for improved robustness in periodic impulsive noise. On the other hand, the proposed system uses convolutional coding, a smaller interleaver across one OFDM symbol, and TFMD modulation. Since modulation diversity does not change data rates, the proposed system has a slightly higher data rates than the reference system, due to the elimination of Reed-Solomon coding. The physical layer parameters for the proposed TFMD system are outlined and compared with those of the reference system in Table II, where a Reed-Solomon code with the input and output block lengths of k_1 and k_2 bytes, respectively, is denoted as k_2/k_1. The Reed-Solomon block sizes and packet sizes in the CENELEC-A and FCC bands are selected according to Table 7-1 and 7-7 in [3]. The effective data rates, excluding the preamble and frame control header, are calculated for the coherent mode.

As described in Section III, the TFMD scheme at the proposed transmitter is parameterized based on the burst structure of the noise and the simulated bandplan. These parameters include the codeword length N_d and $(\Delta K, \Delta T)$ that determine the time-frequency mapping as shown in Fig. 4. To determine ΔT, we assume that the burst duration within a period of the noise, i.e., maximum number of OFDM symbols affected by a burst, is perfectly known at the transmitter. Robustness of the TFMD scheme to estimation error in noise burst duration will be deferred to future study. In either realistic or synthetic noise, each period contains a single burst that extends approximately 4 OFDM symbols in the CENELEC-A band, and 12 OFDM symbols in the FCC band. Therefore we set $\Delta T = 4$ or 12 depending on the bandplan. Given ΔT, the choice of N_d is affected by the packet size. In the FCC band, a smaller packet size is used in our simulations. Without Reed-Solomon coding, each packet only contains 25 OFDM symbols (excluding the reference symbol in non-coherent mode). With $N_d = 3$, it is impossible to guarantee that the 3 components of a codeword are separated from each other by at least 12 OFDM symbols. In the worst case, a single noise burst spans almost half of the packet, and with insufficient separation in time, it is very likely that more than one components of a codeword are contaminated by noise bursts, which leads to performance degradation. As such, only $N_d = 2$ is adopted in the FCC band. In the CENELEC-A band, however, each packet contains 112 OFDM symbols, and hence a separation of at least 4 OFDM symbols can be ensured with both $N_d = 2$ and 3. For a given N_d, ΔK is simply set to be $\lfloor N_{\text{data}}/N_d \rfloor$. An extreme case that is not included in the simulations is when the packet duration is shorter than a noise burst. As mentioned in Section I, this is deferred to future work.

A diversity receiver with either offline or semi-online noise power estimation is used to decode the TFMD signal. In both non-coherent and coherent modes, the offline noise power estimation is performed once for all simulated packets, based on 10 periods of noise samples. In practice, the offline estimates need to be updated once in a while (e.g. on an hourly basis), since the cyclostationary noise statistics is in general slowly varying during the day. Collection of 10 periods of noise samples requires only $83.3\ ms$ of idle time (i.e., when no PLC devices are transmitting within the network), which in general will not be a problem given that the estimation does not need to be updated frequently. In coherent mode, the semi-online estimator can be applied as well. In this case, the estimator first determines the partition of stationary intervals based on 2 periods of noise samples. The entire receiver is then set to run 5 iterations for each packet.

In synthetic noise, the proposed and reference systems are simulated in both the CENELEC-A and FCC bands. In either band, the BER performance is evaluated for both coherent and non-coherent modes. As shown in Fig. 7, the TFMD system achieves significant performance improvement compared to the reference in both operating modes and in both bands. In particular, to achieve the target BER of 10^{-4}, the TFMD system requires considerably lower E_b/N_0 than the reference system. In coherent mode, our proposed transceiver methods obtain up to 6.5 dB gain in the CENELEC-A band, and up to 2.5 dB gain in the FCC band. In non-coherent mode, even larger gains (up to 8 dB in CENELEC-A and 3 dB in FCC) are observed. This indicates that the proposed methods are able to compensate part of the performance gap between non-coherent and coherent schemes. It is noticed that the proposed algorithms offer larger gains in the CENELEC-A band than in the FCC band, since a wide region in the latter band exhibits much lower noise levels. In the CENELEC-A band, increasing N_d from 2 to 3 brings additional 2–3 dB gains when the offline noise power estimator is used. Although the offline estimator consistently outperforms the semi-online alternative, it is observed that the E_b/N_0 gap between the two remains below 2 dB and becomes smaller as N_d increases. In the situations where the offline noise power estimator is infeasible due to limited idle time in the shared PLC channel, the semi-online estimator can still provide significant performance improvement, especially for larger N_d.

The performance improvement of our proposed methods is further validated in realistic noise measurement. In this case, we evaluate the BER performance in the CENELEC-A and FCC bands, but only for coherent mode due to space limit (Fig. 8). With $N_d = 2$, up to 4 dB and 2.5 dB E_b/N_0 gains are achieved in the CENELEC-A and FCC bands, respectively, similarly to those observed in synthetic noise. On the other hand, discrepancies between the BER performance in realistic noise and that in synthetic noise are observed. In the CENELEC-A band, the additional gains by increasing N_d from 2 to 3 are smaller than those in synthetic noise. In realistic noise, compared to the reference system, the TFMD scheme with semi-online noise power estimation exhibits a less rapid BER decrease at higher SNRs. These discrepancies are primarily due to the correlation between the frequency

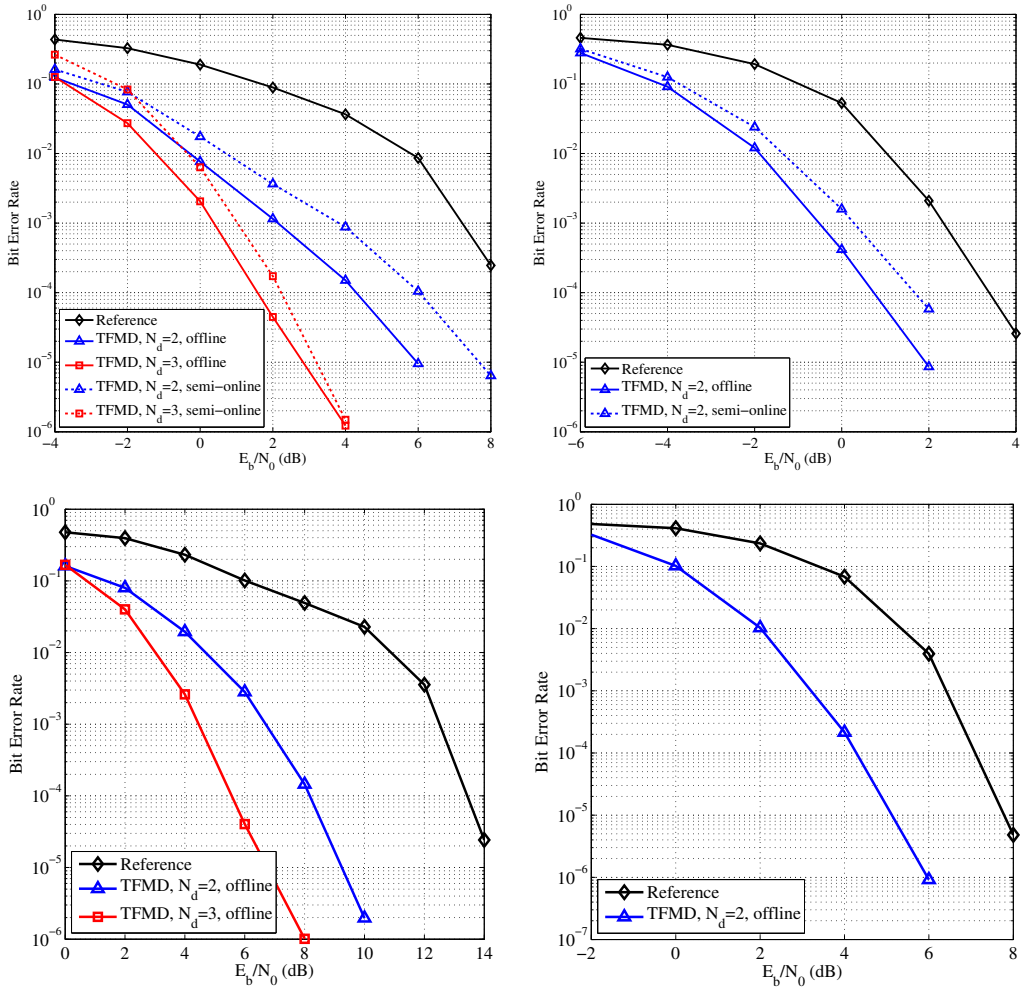

Fig. 7. Bit error rate performance of the proposed TFMD transceiver in periodic impulsive noise generated from a cyclostationary noise model [5], [6]. Performance is evaluated for the coherent mode (top) and the non-coherent mode (bottom), in the CENELEC-A band (left) and the FCC band (middle), respectively. In realistic noise, simulation is only run in the CENELEC-A band (right). For comparison, the reference narrowband PLC system ("Reference") use Reed-Solomon and convolutional coding, whole-packet interleaving and DBPSK/BPSK modulation. The simulated TFMD system ("TFMD") does not use Reed-Solomon coding, and uses a smaller interleaver across one OFDM symbol. N_d denotes the length of modulation diversity codewords. "Offline" and "semi-online" refer to the noise power estimation algorithms.

components of realistic noise, which however is not captured by the LPTV system model [6] and hence not present in synthetic noise. An approximation made in the derivation of the soft-output diversity demodulator and the prior adopted by the TMSBL algorithm is that the frequency components of the noise are mutually uncorrelated. When noise is significantly correlated in frequency domain, such approximation will lead to performance degradation for the TFMD schemes.

For clarity purposes, the E_b/N_0 gains of the proposed system over the reference in both synthetic and realistic noise are summarized and compared in Table III. To summarize, in our simulations, the TFMD transceiver demonstrates enhanced robustness over conventional narrowband PLC systems in both CENELEC-A and FCC bands, and in both non-coherent and coherent modes. The improved reliability is achieved in parallel with slightly increased data rates due to the elimination of Reed-Solomon coding.

TABLE III

E_b/N_0 GAINS IN DB OF THE PROPOSED TFMD SYSTEM OVER THE REFERENCE SYSTEM, MEASURED IN SYNTHETIC AND REASLITIC NOISE, IN CENELEC-A (CEN-A) AND FCC BANDS, AND IN COHERENT (COH) AND DIFFERENTIAL (DIFF) MODES.

TFMD Settings		**Simulated Scenarios**					
		Synthetic Noise				Realistic Noise	
		CEN-A		FCC		CEN-A	FCC
		coh	diff	coh	diff	coh	coh
$N_d = 2$	Offline	4	5	2.5	3	4	2.5
	Semi-online	2	-	1.5	-	2	2
$N_d = 3$	Offline	6.5	8	-	-	4.5	-
	Semi-online	6	-	-	-	4	-

B. Implementation Complexity

In addition to the superior communication performance, our proposed transceiver methods also allow lower-complexity implementation compared to the reference narrowband PLC system. With TFMD, the entire transceiver can be relieved from Reed-Solomon coding/decoding and whole-packet interleaving/deinterleaving, both of which are known to be computationally intensive and memory consuming. This will

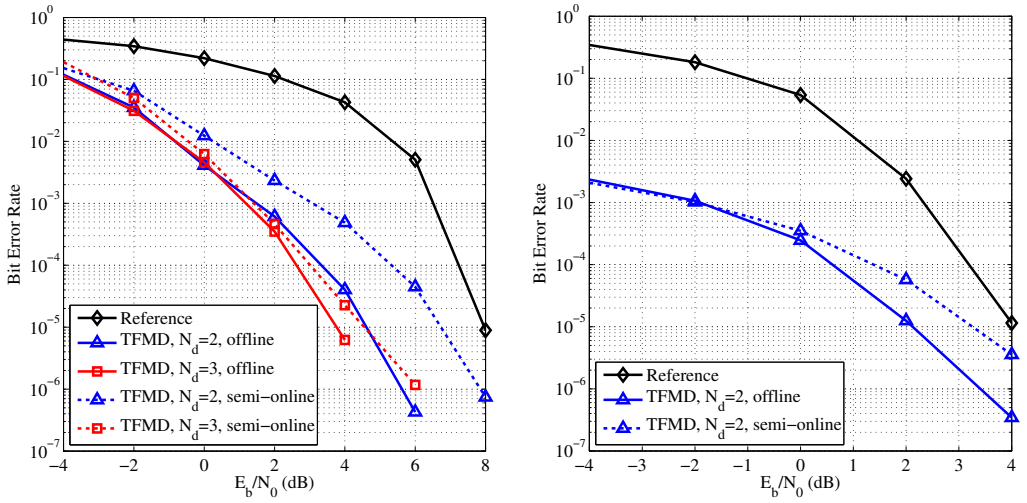

Fig. 8. Bit error rate performance of the proposed TFMD transceiver in realistic noise measured from an outdoor low-voltage power line [6]. Performance is evaluated for the coherent mode in the CENELEC-A band (left) and the FCC band (right). Legend definitions are the same as in Fig. 7.

directly lead to a transmitter that is more power-efficient and cost-effective. The extra complexity introduced by the noise power estimation algorithms can be well compensated by the savings from the Reed-Solomon coding/decoding and the whole-packet interleaving/deinterleaving.

The offline noise power estimator involves a sliding FFT operation over ten periods of noise samples. The sliding FFT is known to have $\mathcal{O}(N_c \log N_c)$ complexity for the first N_c-point FFT, and linear complexity after that. As mentioned previously, the estimates need to be updated once in a while (e.g. on an hourly basis). The overall computational complexity and memory requirement of the offline noise power estimation is much lower compared to the polynomial complexity of the state-of-the-art Reed-Solomon decoders [33]. For the same reason, the diversity receiver with offline noise power estimation has reduced processing latency compared to the reference receiver.

In coherent systems, compared with the offline noise power estimator, the semi-online alternative has a higher complexity, which primarily resides in the T-MSBL algorithm. Standard implementation of the T-MSBL algorithm requires $\mathcal{O}(MN^2)$ additions/multiplications per iteration, where $M \leq 30, N \leq 286$ according to the ITU-T G.9903 standard. The complexity per iteration is comparable with that of the Reed-Solomon decoder, whose complexity is typically in proportion to the third power of the code block length [33], [34] (251 in the CENELEC-A band and 125 in the FCC band). Due to the iterative nature of the algorithm, the overall complexity and latency of the proposed receiver with semi-online noise power estimation might increase by about 10x compared to that of the conventional receiver, assuming 5 iterations for each packet, and 2 noise power spectrums to be estimated. Therefore, such receiver algorithm is more suitable for the data concentrators, which generally have less stringent requirements on power consumption and implementation costs. In fact, the semi-online estimation is mostly needed at the data concentrator, since it sees transmissions from all smart meters within the network and hence has limited idle time. A smart meter, on the other hand, is only affected by transmissions from a few nearby PLC devices. Therefore, it generally experiences a longer idle time which allows collecting enough noise samples for the offline noise power estimation.

VII. Conclusion

This paper proposes a time-frequency diversity modulation scheme to enhance the communication reliability of narrowband PLC systems in periodic impulsive noise. The time-frequency modulation diversity transmitter jointly encodes multiple bits to multiple PSK symbols, and allocates them to different subcarriers in various OFDM symbols. The receiver linearly combines signals received from corresponding sub-channels / OFDM symbols with weights inversely proportional to the sub-channel SNRs. The periodically varying noise power spectrum can be estimated before or during data transmission using sparse Bayesian learning techniques. We validate the proposed transceiver methods based on both realistic noise measurements and synthetic periodic impulsive noise that is emulated from a statistical noise model specified in the IEEE 1901.2 narrowband PLC standard.

Appendix
Derivation of the EM Update Rules for $\boldsymbol{\gamma}$ and $\mathbf{B}$

Given the hierarchical prior formed by (10), (11) and (9), the MAP estimation of $\boldsymbol{\theta} \triangleq \{\boldsymbol{\gamma}, \mathbf{B}, \lambda\}$ can be computed iteratively by the EM algorithm. Following similar routines as in [31], the derivation involves three major steps: (1) transform the MMV model into a higher dimensional SMV model; (2) derive the EM algorithm for the SMV model; and (3) back map the algorithm to the original lower dimensional space. While the same procedure as described in [31] can be directly applied in the first and the last steps, the maximization step in the EM algorithm needs to be derived separately, since the cost function now involves the additional hyperparameters $\mathbf{a}, \mathbf{b}, \mu$ and $\boldsymbol{\Psi}$.

According to [31], in the high dimensional space, the SMV model and the prior (9) can be expressed as

$$\begin{aligned} \bar{\mathbf{y}} &= \mathbf{D}\bar{\mathbf{x}} + \bar{\mathbf{v}}, \\ p(\bar{\mathbf{x}}; \boldsymbol{\gamma}, \mathbf{B}) &= \mathcal{CN}(\bar{\mathbf{x}}; \mathbf{0}, \boldsymbol{\Sigma}_0), \end{aligned}$$

where $\bar{\mathbf{y}} \triangleq \text{vec}(\mathbf{Y}^T), \bar{\mathbf{x}} \triangleq \text{vec}(\mathbf{X}^T), \bar{\mathbf{v}} \triangleq \text{vec}(\mathbf{V}^T)$, $\mathbf{D} \triangleq \boldsymbol{\Phi} \otimes \mathbf{I}_L$, and $\boldsymbol{\Sigma}_0 \triangleq \text{diag}\{\boldsymbol{\gamma}\} \otimes \mathbf{B}$.

The EM algorithm treats $\bar{\mathbf{x}}$ as latent variables, and seeks to maximize the cost function

$$\begin{aligned} Q(\boldsymbol{\theta}) &= \mathbb{E}_{\bar{\mathbf{x}}|\bar{\mathbf{y}};\boldsymbol{\theta}^{(\text{old})}} \Big\{ \log \big[p(\bar{\mathbf{y}}, \bar{\mathbf{x}}|\boldsymbol{\theta}) p(\boldsymbol{\theta}) \big] \Big\} \\ &= \mathbb{E}_{\bar{\mathbf{x}}|\bar{\mathbf{y}};\boldsymbol{\theta}^{(\text{old})}} \big[\log p(\bar{\mathbf{y}}|\bar{\mathbf{x}}, \boldsymbol{\theta}) \big] + \\ &\quad \mathbb{E}_{\bar{\mathbf{x}}|\bar{\mathbf{y}};\boldsymbol{\theta}^{(\text{old})}} [\log p(\bar{\mathbf{x}}|\boldsymbol{\gamma}, \mathbf{B})] + \\ &\quad \log p(\boldsymbol{\gamma}) + \log p(\mathbf{B}), \end{aligned} \tag{16}$$

where $\boldsymbol{\theta}^{(\text{old})}$ denotes the estimate of $\boldsymbol{\theta}$ from the previous iteration. Since the only term in (16) that depends on λ is the first term, the update rule for λ remains the same as in the original T-MSBL algorithm. To derive the update rules for $\boldsymbol{\gamma}$ and $\mathbf{B}$, the cost function (16) can be simplified to

$$\begin{aligned} Q(\boldsymbol{\gamma}, \mathbf{B}) &= \mathbb{E}_{\bar{\mathbf{x}}|\bar{\mathbf{y}};\boldsymbol{\theta}^{(\text{old})}} [\log p(\bar{\mathbf{x}}|\boldsymbol{\gamma}, \mathbf{B})] + \\ &\quad \log p(\boldsymbol{\gamma}) + \log p(\mathbf{B}) \\ &= \tilde{Q}(\boldsymbol{\gamma}, \mathbf{B}) + \log p(\boldsymbol{\gamma}) + \log p(\mathbf{B}), \end{aligned} \tag{17}$$

where $\tilde{Q}(\boldsymbol{\gamma}, \mathbf{B})$ is the simplified cost function used in the original T-MSBL algorithm (Eq. (10) in [31]). Compared to the orignal T-MSBL algorithm, the cost function now involves the hyper-priors (10) and (11) in the two additional terms. We replace $p(\boldsymbol{\gamma})$ and $p(\mathbf{B})$ by the probability density function of the inverse Gamma and the inverse Wishart distributions, respectively

$$\log p(\boldsymbol{\gamma}) \propto \sum_{i=1}^{N} \big[-a_i \log \gamma_i - b_i/\gamma_i \big] \tag{18}$$

$$\log p(\mathbf{B}) \propto -\frac{\mu + L}{2} \log |\mathbf{B}| - \frac{1}{2} \text{Tr}(\boldsymbol{\Psi} \mathbf{B}^{-1}), \tag{19}$$

and take the derivative of (17) with respect to $\gamma_i, \forall i = 1, \cdots, N$

$$\frac{\partial Q}{\partial \gamma_i} \propto \frac{\partial \tilde{Q}}{\partial \gamma_i} - \frac{a_i + 1}{\gamma_i} + \frac{b_i}{\gamma_i^2}, \tag{20}$$

where $\frac{\partial \tilde{Q}}{\partial \gamma_i}$ can be evaluated as in Eq. (11) in [31]. Setting the derivative to zero, we obtain the update rule for γ_i:

$$\gamma_i \leftarrow \frac{\text{Tr}\big[\mathbf{B}^{-1} (\boldsymbol{\Sigma}_{\bar{\mathbf{x}},i} + \boldsymbol{\mu}_{\bar{\mathbf{x}},i} \boldsymbol{\mu}_{\bar{\mathbf{x}},i}^*) \big] + 2b_i}{L + 2a_i}. \tag{21}$$

Similarly, we take the derivative of (17) over $\mathbf{B}$

$$\frac{\partial Q}{\partial \mathbf{B}} = \frac{\partial \tilde{Q}}{\partial \mathbf{B}} - \frac{\mu + L}{2} \mathbf{B}^{-1} + \frac{1}{2} \mathbf{B}^{-1} \boldsymbol{\Psi}^* \mathbf{B}^{-1}. \tag{22}$$

Setting the derivative to zero gives the update rule for $\mathbf{B}$:

$$\mathbf{B} \leftarrow \frac{1}{N + \mu + L} \left[\sum_{i=1}^{N} \frac{1}{\gamma_i} (\boldsymbol{\Sigma}_{\bar{\mathbf{x}},i} + \boldsymbol{\mu}_{\bar{\mathbf{x}},i} \boldsymbol{\mu}_{\bar{\mathbf{x}},i}^*) + \boldsymbol{\Psi}^* \right]. \tag{23}$$

The update rules in (21) and (23) can be back mapped to the original space, as in [31], which results in (14) and (15).

REFERENCES

[1] G. Bumiller, L. Lampe, and H. Hrasnica, "Power line communication networks for large-scale control and automation systems," *IEEE Comm. Magazine*, vol. 48, no. 4, pp. 106–113, 2010.

[2] "G.9902 : Narrowband orthogonal frequency division multiplexing power line communication transceivers for ITU-T G.hnem networks," 2012. [Online]. Available: http://www.itu.int/rec/T-REC-G.9902

[3] "G.9903 : Narrowband orthogonal frequency division multiplexing power line communication transceivers for G3-PLC networks," 2014. [Online]. Available: http://www.itu.int/rec/T-REC-G.9903

[4] "G.9904 : Narrowband orthogonal frequency division multiplexing power line communication transceivers for PRIME networks," 2012. [Online]. Available: http://www.itu.int/rec/T-REC-G.9904

[5] "IEEE standard for low-frequency (less than 500 kHz) narrowband power line communications for smart grid applications," 2013. [Online]. Available: http://standards.ieee.org/findstds/standard/1901.2-2013.html

[6] M. Nassar, A. Dabak, I. Kim, T. Pande, and B. L. Evans, "Cyclostationary noise modeling in narrowband powerline communication for smart grid applications," *Proc. IEEE Int. Conf. on Acoustics, Speech and Signal Process.*, pp. 3089–3092, 2012.

[7] M. Katayama, T. Yamazato, and H. Okada, "A mathematical model of noise in narrowband power line communication systems," *IEEE J. Sel. Areas Comm.*, vol. 24, no. 7, pp. 1267–1276, 2006.

[8] K. F. Nieman, J. Lin, M. Nassar, K. Waheed, and B. L. Evans, "Cyclic spectral analysis of power line noise in the 3-200 kHz band," in *Proc. IEEE Int. Symp. Power Line Comm. and Appl.*, 2013.

[9] M. Nassar, J. Lin, Y. Mortazavi, A. Dabak, I. H. Kim, and B. L. Evans, "Local utility power line communications in the 3-500 kHz band: Channel impairments, noise, and standards," *IEEE Signal Process. Magazine*, vol. 29, no. 5, pp. 116–127, 2012.

[10] J. Lin, M. Nassar, and B. L. Evans, "Impulsive noise mitigation in powerline communications using sparse Bayesian learning," *IEEE Journal on Selected Areas in Comm.*, no. 7, pp. 1172–1183, 2013.

[11] R. García, L. Díez, J. Cortes, and F. Canete, "Mitigation of cyclic short-time noise in indoor power-line channels," *Proc. IEEE Int. Symp. Power Line Comm. and Appl.*, pp. 396–400, 2007.

[12] A. Liano, A. Sendin, A. Arzuaga, and S. Santos, "Quasi-synchronous noise interference cancellation techniques applied in low voltage PLC," *Proc. IEEE Int. Symp. Power Line Comm. and Appl.*, 2011.

[13] J. Lin and B. L. Evans, "Cyclostationary noise mitigation in narrowband powerline communications," *Proc. APSIPA Annual Summit Conf.*, 2012.

[14] R. Schober, L.-J. Lampe, W. H. Gerstacker, and S. Pasupathy, "Modulation diversity for frequency-selective fading channels," *IEEE Trans. Info. Theory*, vol. 49, no. 9, pp. 2268–2276, 2003.

[15] B. M. Hochwald and T. L. Marzetta, "Unitary space-time modulation for multiple-antenna communications in rayleigh flat fading," *IEEE Trans. Info. Theory*, vol. 46, no. 2, pp. 543–564, 2000.

[16] A. Al-Dweik, A. Hazmi, B. Sharif, and C. Tsimenidis, "Efficient interleaving technique for ofdm system over impulsive noise channels," in *IEEE Int. Symp. Personal Indoor and Mobile Radio Comm.* IEEE, 2010, pp. 167–171.

[17] S. Nayyef, C. Tsimenidis, A. Al-Dweik, B. Sharif, and A. Hazmi, "Time- and frequency-domain impulsive noise spreader for OFDM systems," in *IEEE Int. Conf. on Trust, Security and Privacy in Computing and Comm.*, 2012, pp. 1856–1861.

[18] Y. Yoo and J. Cho, "Asymptotic analysis of CP-SC-FDE and UW-SC-FDE in additive cyclostationary noise," *Proc. IEEE Int. Conf. Comm.*, pp. 1410–1414, 2008.

[19] L. Lampe, "Bursty impulse noise detection by compressed sensing," *Proc. IEEE Int. Symp. Power Line Comm. and Appl.*, pp. 29–34, 2011.

[20] M. Tipping, "Sparse bayesian learning and the relevance vector machine," *J. Mach. Learn. Res.*, vol. 1, pp. 211–244, 2001.

[21] J. Boutros and E. Viterbo, "Signal space diversity: a power-and bandwidth-efficient diversity technique for the Rayleigh fading channel," *IEEE Trans. Info. Theory*, vol. 44, no. 4, pp. 1453–1467, 1998.

[22] B. M. Hochwald and W. Sweldens, "Differential unitary space-time modulation," *IEEE Trans. Comm.*, vol. 48, no. 12, pp. 2041–2052, 2000.

[23] A. Batra and J. Balakrishnan, "Improvements to the multi-band OFDM physical layer," in *Consumer Comm. and Networking Conf.*, vol. 2. IEEE, 2006, pp. 701–705.

[24] S. Galli, "A novel approach to the statistical modeling of wireline channels," *IEEE Trans. Comm.*, vol. 59, no. 5, pp. 1332–1345, 2011.

[25] A. Dabak, I. H. Kim, and T. Pande, "Channel modeling of medium to low voltage links for AMI applications of PLC," 2012. [Online]. Available: http://www.ti.com/lit/wp/spry202/spry202.pdf

[26] V. Pauli, L. Lampe, and R. Schober, "Turbo DPSK using soft multiple-symbol differential sphere decoding," *IEEE Trans. Info. Theory*, vol. 52, no. 4, pp. 1385–1398, 2006.
[27] D. Divsalar and M. K. Simon, "Multiple-symbol differential detection of mpsk," *IEEE Trans. Comm.*, vol. 38, no. 3, pp. 300–308, 1990.
[28] R. Schober, W. H. Gerstacker, and J. B. Huber, "Decision-feedback differential detection of MDPSK for flat Rayleigh fading channels," *IEEE Trans. Comm.*, vol. 47, no. 7, pp. 1025–1035, 1999.
[29] J.-M. Bohli, C. Sorge, and O. Ugus, "A privacy model for smart metering," in *IEEE Int. Conf. on Comm. Workshops,*, 2010, pp. 1–5.
[30] S. Galli, A. Scaglione, and Z. Wang, "For the grid and through the grid: The role of power line communications in the smart grid," *Proc. of the IEEE*, vol. 99, no. 6, pp. 998–1027, 2011.
[31] Z. Zhang and B. D. Rao, "Sparse signal recovery with temporally correlated source vectors using sparse Bayesian learning," *IEEE Journal of Selected Topics in Signal Processing*, vol. 5, no. 5, pp. 912–926, 2011.
[32] D. Wipf and B. Rao, "Sparse Bayesian learning for basis selection," *IEEE Trans. Signal Process.*, vol. 52, no. 8, pp. 2153–2164, 2004.
[33] Y. Cassuto, J. Bruck, and R. J. McEliece, "On the average complexity of Reed–Solomon list decoders," *IEEE Trans. on Info. Theory,*, vol. 59, no. 4, pp. 2336–2351, 2013.
[34] R. G. Gallager, *Information theory and reliable communication*. Springer, 1968, vol. 2.

Jing Lin (jslin@qti.qualcomm.com) received the B.S. degree in electrical engineering from Tsinghua University, China, in 2008, and the M.S. and PhD degrees in electrical and computer engineering from the University of Texas at Austin, in 2010 and 2014, respectively. She is currently with Qualcomm Technologies, Inc., where she is working as a senior system engineer on 4G LTE modem design. Her research interests include signal processing algorithms and implementations with applications in wireless and powerline communications.

Tarkesh Pande received his BSEE, MSEE, and Ph.D. degrees in electrical engineering from Purdue University in 1999, 2003 and 2006 respectively. Since 2007 he has been with the EP R&D center at Texas Instruments Inc. in Dallas, USA. His research interests are in wireless and wireline communications, intelligent transportation systems and sensors based signal processing.Dr. Pande is a senior member of the IEEE and is a member of Eta Kappa Nu.

Il Han Kim received the B.S. and M.S. degrees in electrical engineering from Korea Advanced Institute of Science and Technology in 2002 and 2004, respectively, and Ph.D. degree in electrical engineering from Purdue University in 2008. During 2004 and 2005, he was with the Electronics and Telecommunications Research Institute, Daejeon, Republic of Korea. During the summers of 2007 and 2008, he was with the DSPS R&D Center, Texas Instruments Incorporated, where he worked on LTE and LTE-Advanced standardization. Since January 2009, he has been with the EP Systems R&D Center, Texas Instruments Incorporated, where he works as a systems engineer on analysis for various communication systems including power line communications (PLC) and ultrasonic communications. His research interests include signal processing algorithms and analysis for various communication systems.

Anuj Batra received his BSEE from Cornell University, MSEE from Stanford University, and Ph.D. from Georgia Institute of Technology. He is a Distinguished Member of Technical Staff at Texas Instruments. He leads and manages the Advanced Communications branch within the Internet of Things Lab. The branch develops algorithms, defines system specifications and drives standards for multiple power line communications (PLC) modems and for multiple physical (PHY) layers on a single software-defined radio modem.

Dr. Batra joined Texas Instruments in 2000 and has worked on both wired and wireless communications, including PLC, co-developing the OFDM PHY for smart utilities networks, co-developing the narrowband PHY for body area networks in IEEE 802.15.6, co-developing the multi-band OFDM (MB-OFDM) PHY for ultra-wideband (UWB) in WiMedia/ECMA, implementing and standardizing Wi-Fi technologies (IEEE 802.11g/n), and standardizing adaptive frequency hopping techniques for Bluetooth.

Dr. Batra has been awarded 85 patents, is a Senior IEEE member, and in 2004, he was named one of the worlds 100 Top Young Innovators by Technology Review, MITs Magazine of Innovation, for his work on developing and championing the MB-OFDM UWB technology.

Brian L. Evans holds the Engineering Foundation Professorship at UT Austin. He earned his BSEECS (1987) degree from the Rose-Hulman Institute of Technology, and his MSEE (1988) and PhDEE (1993) degrees from the Georgia Institute of Technology. From 1993 to 1996, he was a post-doctoral researcher at the University of California, Berkeley. In 1996, he joined the faculty at UT Austin.

Prof. Evans research bridges the gap between digital signal processing theory and embedded real-time implementation. His research interests include wireless interference mitigation, smart grid communications, smart phone video acquisition, multicore computing. and cloud radio access networks.

Prof. Evans has published more than 220 refereed conference and journal papers, and graduated 25 PhD and 9 MS students. He received the Best Paper Award at the 2013 IEEE Int. Symp. on Power Line Communications and Its Applications, and a Top 10% Paper Award at the 2012 IEEE Multimedia Signal Processing Workshop. He has received three teaching awards at UT Austin: Gordon T. Lepley Memorial ECE Teaching Award (2008), Texas Exes Teaching Award (2011) and HKN Outstanding ECE Professor (2012). He received a 1997 US National Science Foundation CAREER Award.